

General Disclaimer

One or more of the Following Statements may affect this Document

- This document has been reproduced from the best copy furnished by the organizational source. It is being released in the interest of making available as much information as possible.
- This document may contain data, which exceeds the sheet parameters. It was furnished in this condition by the organizational source and is the best copy available.
- This document may contain tone-on-tone or color graphs, charts and/or pictures, which have been reproduced in black and white.
- This document is paginated as submitted by the original source.
- Portions of this document are not fully legible due to the historical nature of some of the material. However, it is the best reproduction available from the original submission.

(NASA-TM-85011) A BALLCON-ECRHF INSTRUMENT
FOR HIGH-RESOLUTION ASTROPHYSICAL
SPECTROSCOPY IN THE 20-8000 KEV ENERGY RANGE
(NASA) 52 p HC A04/MF A01 CSCI 14B

#83-23573

Unclass
11604

G3/35



Technical Memorandum 85011

A Balloon-Borne Instrument for High-Resolution Astrophysical Spectroscopy in the 20-8000 keV Energy Range

W. Paciesas, R. Baker, D. Boclet, S. Brown,
T. Cline, H. Costlow, P. Durouchoux, C. Ehrmann,
N. Gehrels, J.M. Hameury, R. Haymes,
B. Teegarden and J. Tueller

APRIL 1983

National Aeronautics and
Space Administration

Goddard Space Flight Center
Greenbelt, Maryland 20771



ORIGINAL PAPER
OF POOR QUALITY

A BALLOON-BORNE INSTRUMENT FOR HIGH-RESOLUTION ASTROPHYSICAL
SPECTROSCOPY IN THE 20-8000 KEV ENERGY RANGE

W. Paciesas^{1,2,6}, R. Baker¹, D. Boclet³, S. Brown¹, T. Cline¹,
H. Costlow¹, P. Durouchoux³, C. Ehrmann¹, N. Gehrels^{1,4},
J. M. Hameury³, R. Haymes⁵, B. Teegarden¹, and J. Tueller^{1,2}

Accepted for publication in Nuclear Instruments and Methods, March 25, 1983

1. NASA/Goddard Space Flight Center, Greenbelt, MD 20771, U.S.A.
2. Also, Department of Physics and Astronomy, University of Maryland, College Park, MD 20742, U.S.A.
3. Centre d'Etudes Nucléaires de Saclay, 91191 Gif-sur-Yvette Cedex, France.
4. NAS/NRC Resident Research Associate
5. Department of Space Physics and Astronomy, Rice University, Houston, TX 77001, U.S.A.
6. Present address: Department of Physics, University of Alabama in Huntsville, Huntsville, AL 35899, U.S.A.

ABSTRACT

The Low Energy Gamma-ray Spectrometer (LEGS), a joint project among NASA/GSFC, CENS, and Rice University, is designed to perform fine energy resolution measurements of astrophysical sources. The instrument can be configured for a particular balloon flight with either of two sets of high-purity germanium detectors. In one configuration, the instrument uses an array of three coaxial detectors (effective volume $\approx 230 \text{ cm}^3$) inside an NaI (Tl) shield and collimator (field-of-view $\approx 16^\circ$ FWHM) and operates in the 80-8000 keV energy range. In the other configuration, three planar detectors (effective area $\approx 53 \text{ cm}^2$) surrounded by a combination of passive Fe and active NaI for shielding and collimation (field-of-view $\approx 5^\circ \times 10^\circ$ FWHM) are optimized for the 20-200 keV energy range. In a typical one-day balloon flight, LEGS sensitivity limit (3σ) for narrow line features is $\leq 8 \times 10^{-4}$ ph/cm²-s (coaxial array: 80-2000 keV) and $\leq 3 \times 10^{-4}$ ph/cm²-s (planar array: 50-150 keV).

1. INTRODUCTION

Spectroscopy stands out as one of the most important techniques which astronomers have used to advance our understanding of the universe. The evolution of the technique from its optical origins to the radio, infrared, ultraviolet, and X-ray regions of the spectrum was crucial in discovering and/or investigating such phenomena as quasars, supernovae, novae, active galaxies, binary stellar systems, the interstellar and intergalactic media, etc. Without spectroscopy our knowledge of the universe would be limited indeed. On the other hand, many of the most scientifically exciting phenomena in the universe involve violent, energetic events from which emission can be detected extending well into the gamma-ray (\gtrsim a few tens of keV) region of the spectrum. It is natural, therefore, that the techniques of gamma-ray spectroscopy should be applied to astrophysics.

Theoretical investigations of the most likely astrophysical sites of gamma-ray line emission have been numerous (reference 1 and references therein), but in practice the observational difficulties have been formidable. Many of the theoretical line flux predictions lie just below the sensitivity limits of present-day instruments. It thus appears likely that even modest improvements in sensitivity may provide interesting new results.

Most of the previous experiments have used scintillation detectors for spectroscopy because of their availability, large size, and relatively low cost. Unfortunately, the poor energy resolution ($\Delta E/E \gtrsim 15$ percent at 60 keV) of scintillators is a fundamental limitation in characterizing both the shape and the energy of the observed features. Higher resolution observations are required in order to provide the crucial theoretical constraints implicit in these parameters. A number of instruments designed specifically for high-resolution gamma-ray spectroscopy have been built and flown on either high-

altitude balloons²⁻⁷ or satellites⁸⁻¹⁰. The Low Energy Gamma-ray Spectrometer (LEGS) described in this paper provides a superior combination of detector size and type, shield thickness, and collimator design which results in significant improvements in sensitivity over most previous instruments. It is unique in that either of two different sets of detectors can be installed prior to a particular flight, depending on the observational objectives. An additional unusual feature is the inclusion of a circuit designed to identify pairs of detector events closely spaced in time, allowing the elimination of certain particle-induced background features at float altitudes.

We describe the LEGS instrument in Section II and discuss its flight performance in Section III. The latter section also includes the results of an effort to explain quantitatively the observed continuum background in the instrument as well as several of the line features. Section IV summarizes the sensitivity of the LEGS in a typical observation.

II. SYSTEM DESCRIPTION

a. General Description

We first give an overall description of LEGS and then elaborate on several important subsystems. A cross-sectional view of the LEGS gondola is shown in Figure 1. A cryostat containing the detector array is the heart of the system and is mounted inside an active anticoincidence shield which consists of ~ 190 kg of NaI scintillator in three sections viewed by a total of 24 photomultiplier tubes. The three sections of the shield fit together in such a way as to provide between 30 and 60 g/cm^2 of NaI between the detectors and non-aperture photons.

The spectrometer and associated electronics (anticoincidence logic, detector and shield pulse height analyzers, digital telemetry encoder, and command distribution system) are enclosed in a sealed aluminum pressure vessel which maintains these subsystems at atmospheric pressure. A stainless steel dewar is mounted in a cage attached below the pressure vessel and holds ~ 25 liters of liquid nitrogen for cooling of the germanium detectors. This is enough to keep the detectors at operating temperature (~ 100 K) for about one week. The thermal interface to the detectors is a copper cold finger enclosed in an evacuated stainless steel jacket. A hole in the rear shield section allows the cold finger to reach the dewar. A gasket around the stainless steel jacket prevents air leakage at the point where the cold finger enters the pressure vessel. The dewar is also sealed to prevent the liquid nitrogen from freezing at float altitude. A pressure relief valve allows boil-off of nitrogen while maintaining approximately one-third atmospheric pressure in the dewar.

Thermal control of the spectrometer is accomplished by encasing the pressure vessel in two inches of ethafoam insulation and by isolating the

pressure vessel from the gondola using epoxy fiberglass bushings at the experiment attachment points. Auxiliary resistance heaters are also available for use in extreme conditions.

The experiment is mounted in an azimuth-elevation configuration in an open-frame gondola consisting of a U-shaped yoke, support arms, and "sidecars." The sidecars are not part of the primary load-bearing structure, but rather function as supports for various gondola subsystems such as batteries and control electronics. The sidecars also provide some shock absorption on landing and are designed to be conveniently repaired and/or replaced.

The attachment points of the pressure vessel constitute the axis about which the telescope is rotated in elevation. The elevation angle is measured using a digital shaft angle encoder coupled directly to one of the pivot points. This pivot point is connected through a gear box to a small DC motor which controls the elevation angle. The experiment can be rotated approximately 60° in either direction from vertical.

Four stainless steel cables connect the corners of the gondola to a single attachment point, above which is a drive motor which rotates the entire gondola in azimuth. The drive motor is a torque-limiting powered swivel containing two sets of thrust bearings supporting two shafts coupled by an outer race. The balloon connects to the top shaft and the instrument connects to the bottom shaft. A small DC motor is attached to the instrument shaft and drives the outer race, thereby developing a torque between the instrument and the balloon. The torque is limited by the break-away torque of the upper bearing and its sliding friction. Azimuth control is accomplished by driving the race clockwise or counter-clockwise at the necessary rate to keep the telescope on target. This system can require several minutes to accomplish

large azimuth changes even when optimum control algorithms are used. Therefore, the ability of the elevation system to operate on either side of vertical is useful. An equivalent change of 180° in azimuth may be accomplished by rotating the telescope in elevation to its complementary value on the opposite side of vertical. The azimuth of the experiment is determined using a cross magnetometer of our own design which is described in Section IIe. Two such units are flown for redundancy, one mounted on a boom at the top of the yoke and one mounted on a sidecar near a corner of the gondola.

Instrument pointing is controlled by an onboard microcomputer based on a Texas Instruments TMS9900 microprocessor. Latitude, longitude, target right ascension, target declination, and local magnetic deviation are entered by telecommand from the ground and the computer periodically calculates and updates the azimuth and elevation of the target and drives the control motors appropriately. The computer handles interpretation and distribution of digital telecommands, including commands to the spectrometer system electronics. The pointing microcomputer is mounted on the sidecars, as are other subsystems which handle power distribution and telecommand interface functions. Lithium batteries capable of supplying approximately 60 hours of operation are also mounted in the sidecars.

Verification of the pointing system performance is accomplished at night using a star camera mounted on the experiment pressure vessel. The motorized camera is a modified version of a Robot model 36 with a Schneider Xenon 50 mm f/1.9 lens. The field-of-view is approximately $30^\circ \times 40^\circ$. A 500 ft. magazine holds enough film for ~ 4000 pictures. Exposures are synchronized to a clock derived from the telemetry encoder, so that rates between one photo per ~ 0.5 s and one photo per ~ 64 s are available in increments of ~ 0.5 s.

A sun-azimuth sensor (mounted on the gondola frame) has been constructed for daytime verification of the pointing. The device is based on the rotating-vane principle, whereby a silicon photodiode whose field-of-view is collimated to a narrow-vertical slit is continuously rotated about a vertical axis. The signal produced in the photodiode as the slit scans across the sun triggers the readout of the scan angle using a 12-bit digital shaft angle encoder. Although it has not yet been used successfully in flight, the device allows, in principle, the determination of the azimuth angle to within approximately 0.2° .

An MKS Baratron^R Type 222A pressure transducer provides data on the pressure altitude in the region between 1 and 12 millibars.

b. Detectors

The LEGS system employs high-purity germanium detectors which, when cooled to liquid nitrogen temperatures, have excellent energy resolution. A novel feature of this instrument is that either of two different arrays of three detectors each may be installed; the choice for a particular flight depends upon the observational goals. Table 1 compares the characteristics of the two arrays. Coaxial p-type detectors have been used in most previous high-resolution instruments. These detectors have a relatively thick Li diffused layer on the outside surface which functions as the n^+ contact. This layer is insensitive to interactions within it and therefore limits the useful gamma-ray energy range of such detectors to ~ 80 keV or higher, well above the practical lower limit of ~ 20 keV which the residual atmosphere imposes on balloon-borne instruments. The attainment of good sensitivity in the region between 20 and 80 keV requires a different type of detector.

In principle, it is possible to reverse the contacts on a p-type detector, but such an arrangement requires much higher bias voltages (~ 5000 v)¹¹. Moreover, such a detector depletes from the inner contact, so that the region where most interactions occur (near the outer surface) has the lowest electric field, an undesirable property. Coaxial detectors made from n-type germanium are a recently developed alternative¹¹. In this case, the placement of the thin p⁺ contact on the outside results in bias voltages and field morphology which are comparable to the normal p-type configuration. The use of this type of detector would have allowed LEGS to cover the 10-8000 keV range in a single configuration. As actually realized, however, the separate LEGS configurations enabled us to optimize the background properties and angular response of the instrument in ways which would have been impractical otherwise.

The LEGS low-energy configuration employs an array of planar detectors made from 1 cm thick slices of germanium on which the flat surfaces are used as contacts. The thin metal surface-barrier cathode is then defined to be the front surface, producing a dead layer which is negligible for our purposes. In this configuration full depletion requires impractically high bias voltages unless the detector thickness is less than ~ 1.5 cm. Although such thin detectors have poor high-energy response, they have the advantage of lower volume-dependent background relative to the coaxial detectors.

Each detector in an array is connected to an independent preamplifier, pulse-shaping amplifier, and 8192-channel pulse-height analyzer. The preamplifiers for both configurations are conventional DC-coupled FET-input designs in which the FET and feedback network are housed inside the cryostat and kept near liquid nitrogen temperature, thereby decreasing the electronics noise. The preamplifiers are modified versions of the model RG-11A made by Princeton Gamma-Tech, Inc. In the planar configuration they are mounted

inside the NaI shield, while they are outside the shield in the coaxial configuration.

The effective area of the detector arrays to incident photons was determined using laboratory measurements with standard radioactive sources, supplemented by Monte Carlo computer simulations. Calibration lines from laboratory sources ranged in energy from 6.4 keV to 2.6 MeV. Response curves thus obtained for the individual detectors in each array were summed together and corrected for finite source distance. The results are displayed in Figure 2. The effect of the dead layers and the cryostat window (and, in the case of the planars, the iron collimator described in Section IIc) have not been removed, so that these curves represent the effective response of the entire system with the exception of small corrections for absorption in the pressure vessel window and the foam insulation. The response due to the single- and double-escape peaks produced when the incident photon interacts via pair production are not significant because the size of the detectors make escape unlikely and because the shield is effective in vetoing most events in which escape occurs. The relative advantage of the planar detectors at low energies and the coaxial detectors at high energies is evident from the figure.

Another, less significant, difference between the two arrays is the energy resolution. Although both are excellent in this respect, the resolution in the planar configuration is generally better due to lower capacitance and more complete charge collection. Laboratory measurements of the energy resolution of individual detectors are included in Table 1; in-flight performance is typically not this good because of practical problems in correcting for gain drifts and combining the results from individual detectors (see Section IIIb).

Although LEGS is primarily designed to look for spectral lines, the continuum spectra of the target sources are also of interest. Besides the full-energy peaks (and the escape peaks), a monoenergetic source produces a continuum of events in which the detected energy is less than the input energy. This arises either from Compton scattered photons which deposit only part of their energy in the detector and do not trigger the anticoincidence shield, or from incomplete charge collection of full-energy loss events. The continuum due to partial energy-loss Compton events was calculated using a Monte Carlo code and verified at several energies using laboratory calibration sources. The continuum due to incomplete charge collection is important primarily at low energies and was measured with laboratory sources. These effects turned out to be significant only for the coaxial array. The results thus obtained are combined with the full energy and escape peak response curves to compile a response matrix which can then be used to determine the best-fitting input spectral parameters of observed sources by the usual χ^2 -minimization techniques.

c. Anticoincidence Shield and Collimator

The cryostat containing the detector array is surrounded by a three-section NaI (Tl) anticoincidence shield which also functions as a collimator, providing a flat-topped field-of-view of 16° FWHM. The rear section of the shield is made from conventional NaI while the two other sections are made from Harshaw Polyscin^R. Since, as discussed in the previous section, the planar array is optimized for the 20-200 keV energy range, it was desirable and feasible to add passive collimation in order to reduce source confusion as well as to decrease the aperture flux component of the detector background. A simplified cutaway diagram comparing the two detector configurations is shown

in Figure 3. The diagram of the planar configuration shows the passive collimators, which consist of three iron tubes each with a single iron slit along the diameter. The inner diameter of the tubes is larger than the detector diameter so that the response parallel to the slit has a flat-topped shape with $\sim 10^\circ$ FWHM. In the direction perpendicular to the slit, the response is nearly triangular with $\sim 5^\circ$ FWHM. This design is tailored to the performance of the servo system. Since the slits are aligned parallel to each other and to the elevation axis of the telescope, the response is sharp along the elevation direction (where the pointing accuracy is good) and has a flat top along the azimuth direction (where errors of $\sim 1^\circ$ can accumulate due to systematic limitations of accuracy and stability). In addition, the use of iron eliminates any background contribution from fluorescence since the iron K-shell X-rays lie well below the detector threshold. A higher-Z material is not necessary because the NaI collimator eliminates gamma-rays arriving at large angles to the collimation axis.

In the coaxial configuration the angular response of each detector is asymmetric because the detectors are not located on the collimator axis. Also, since the detectors are much smaller in diameter than the collimator, the response curve has a broad, flat top. The effects tend to be smoothed out, however, when the detectors are summed. Figure 4a shows the summed response for two extreme cases. The curves are derived by adjusting the parameters of an approximate numerical calculation to fit laboratory measurements of the 662 keV full-energy peak from ^{137}Cs . The resulting response has an FWHM $\approx 16^\circ$ with minor ($\leq 1^\circ$) deviations from symmetry as a function of azimuth angle around the collimator axis. Similar measurements at 1173 and 1332 keV also agree well with these curves except in the wings where the 662 keV data predict less than about 20 percent exposure. This effect is

shown by the short-dashed lines in Figure 4a. The same conclusion also applies to the Compton continuum from all three lines: i.e., the angular response is consistently higher than the 662 keV full-energy peak response in the wings below 20 percent but agrees well otherwise. This relatively weak energy dependence of the angular response simplifies data analysis substantially.

The angular response of the planar configuration is illustrated in Figure 4b. This case differs from the coaxial case in that the azimuthal asymmetry in the response of the individual detectors does not average out when the detectors are summed. Thus Figure 4b represents both the individual detector response and the summed array response. The azimuthal asymmetry changes the shape of the response from a relatively sharp triangle with 5° FWHM in the (gondola) elevation direction to a trapezoidal shape with 2° full width at 95 percent transmission and 10° FWHM in the (gondola) azimuth direction. This response has been verified with laboratory sources to be essentially energy independent below ~ 400 keV.

d. Instrument Electronics and Data-Handling System

A functional block diagram of the instrument electronics is shown in Figure 5. The output of each detector preamplifier is connected to one of three Canberra 2011 spectroscopy amplifiers. The prompt bipolar output of each spectroscopy amplifier is sent to threshold circuits for use in event selection logic. In the usual fashion, the occurrence of an event which falls between two preset energy thresholds triggers a gate which determines the presence or absence of a simultaneous event in the anticoincidence shield. Unless the system is busy with previous analysis, the absence of a shield event causes pulse-height analysis of the signal at the delayed unipolar

output of the spectroscopy amplifier. Each detector has its own Tracor Northern NS623 8192-channel ADC for pulse-height analysis. The results are then stored in a two-level buffer for eventual transmission to the ground via telemetry. These are called high-priority events. An event which satisfies the detector threshold criteria but is vetoed by the guard anticoincidence may still be analyzed and transmitted if there is no high-priority event awaiting transmission. Such events are called low-priority and are tagged.

Two types of pulse-height analysis of the shield events are performed: a) events coincident with detector events are analyzed with 6-bit accuracy and encoded in the telemetry stream in the same block as the detector events. Control of the linear gate for this analysis is provided solely by the lower detector threshold, so that these data may be used in post-flight analysis to provide a lower anticoincidence shield threshold if desired. In practice, electronic noise problems in the linear gate have precluded use of this technique in previous flights; b) shield events are also analyzed on a first-in, first-out basis, independent of the detector events, and encoded in the telemetry with 6-bit accuracy. These data are used to monitor the spectrum in the shield during the flight and are also useful in ground calibration.

Encoding of the data into the telemetry format is performed by a custom-built Digital Processor Unit (DPU). The telemetry format uses a minor frame consisting of 128 16-bit words. One hundred twelve of these words are used for the detector events, each of which occupies a block of four words. An event block normally contains a 13-bit event pulse height, four 6-bit shield pulse heights (two of each type described above), 11 bits of fine timing information (which enables determination of the arrival time of each event to a precision of 100 μ s), and 11 bits identifying the event priority type,

originating detector, and originating shield section for the analyzed shield events. Detection of events in two detectors simultaneously causes two of the shield pulse height words to be overwritten with the second detector pulse height. The remaining bits in the event block have been used for various diagnostic information in the coaxial configuration and contain the pulse-pair timing (PPT) information when the planar detectors are used.

The PPT circuit is a special purpose circuit which was developed in an effort to eliminate certain background spectral features caused by neutron activation of the detectors at float altitudes. In particular, there is a complex feature between 54 and 67 keV produced by neutron activation of ^{72}Ge . This interaction produces the daughter nucleus ^{73}Ge in an excited, metastable state which decays through an intermediate level, producing photons at 54 and 13 keV. The intermediate level has a half-life of $\sim 3 \mu\text{s}$ ¹² which is comparable to the resolving time of the LEGS pulse-height analysis system. Therefore, lines at 54 keV and 67 keV (the sum peak) show up in the background spectrum together with a continuum of events of intermediate energy. Since these features occur in a region of particular interest because of the reported cyclotron feature around 60 keV in Her X-1¹³, it was deemed useful to discriminate against this activation background as much as possible.

The resulting circuit employs a system of fast amplifiers which are connected directly to the detector preamplifiers at a point prior to integration of the pulse. The output of these fast amplifiers is used to trigger discriminators which have a threshold of ~ 10 keV. The PPT circuit scales the time between consecutive fast threshold signals up to a maximum value of 90 μs . When an event triggers the analysis threshold, the PPT time is stored. When the event has been analyzed ($\sim 100 \mu\text{s}$ later), the PPT circuit is interrogated again and the value stored. The smaller of these two values

is transmitted as a 3-bit logarithmic time with the event. This time corresponds to the time between the event and the fast threshold signal nearest that event, regardless of whether the signal was before or after the analyzed event. The minimum time resolution of the PPT discriminators is limited to 0.8 μ s by the shaping necessary to eliminate interference problems on the fast thresholds. In-flight performance of the PPT circuit is described in Section IIIb.

The remaining 16 words of a minor frame contain various housekeeping and pointing information. The content of these words is cycled within a major frame of 64 minor frames. Information transmitted includes: a) raw experiment rates and deadtime information; b) system voltage monitors; c) temperature sensors; d) pointing parameters; e) experiment status information; f) readout of auxiliary level sensors, pressure sensors, and Sun azimuth sensor; g) coarse timing information; and h) command verification.

Timing on the gondola is controlled by a custom-built flight time standard based on an Austron model 1105-2 precision quartz oscillator. The module also includes a frequency countdown register, time code generator/reader, time processing and output logic, and a power conditioner. The standard can be set by any time code generator capable of providing either NASA 36-bit or IRIG time code and a synchronization pulse once per second. Calendar time accurate to 0.1 ms and with a cycle time of two days is provided by the time standard and encoded in the telemetry once per minor frame. In addition, the telemetry bit clock (nominally 10 kHz) is derived from the time standard.

e. Pointing Control System

Pointing of the instrument is controlled by an onboard microcomputer; a block diagram of the system is shown in Figure 6. The system is built around a TM990/100M microcomputer consisting of a TMS9900 microprocessor with 512 16-bit words of RAM and 4096 words of EPROM. One RS-232 CRT interface is provided for status output and debug control. During the flight, these data are returned on a separate analog subcarrier which can be used for prompt monitoring of microcomputer functions independently of the main data stream. A digital housekeeping output port also transmits certain microcomputer status information to the DPU for inclusion in the main data stream. Sixteen quantities are subcommutated with a cycle time of ~ 13.1 s at the normal telemetry rate.

The main functions of the pointing system electronics are: a) compute the azimuth and elevation of the target given the experiment latitude and longitude, the right ascension and declination of the target, and the time of day; b) point the experiment to the computed azimuth and elevation by measuring the actual azimuth and elevation and driving control motors appropriately; c) interpret commands from the telecommand decoder and distribute these as required to the LEGS subsystems; and d) provide pointing system status information to the DPU for encoding in the telemetry data stream.

Azimuth and elevation calculations are based on standard formulae. Latitude, longitude, right ascension, and declination are entered into the computer by telecommand; updating of the latitude and longitude is usually performed once per half-hour in order to maintain better than 0.1° accuracy in the calculations. Day-of-year and time-of-day are derived from an internal battery-powered clock which is set before the flight; the timer may be reset

by telecommand in flight if desired. These calculations are updated every 4.9984 s.

The microcomputer controls the elevation and azimuth through two essentially similar servo drive circuits. The drive rate is controlled by varying the duty cycle of a train of constant-voltage stepping pulses. Every 0.1 s the desired values of elevation and azimuth are subtracted from the current values to find the elevation error and the azimuth error. Also, the previous azimuth is subtracted from the current azimuth to measure the azimuth drift rate. The motor drive rates are then adjusted according to a set of algorithms which have been optimized empirically for the LEGS system. An important feature of the microcomputer is the ability to modify the parameters of the pointing algorithms in flight by telecommand. This allows real-time compensation for changes in mechanical characteristics due to thermal or other flight-related stresses.

The experiment elevation angle is measured using a Baldwin Electronics, Inc. model 5VN241BGL 12-bit binary shaft encoder coupled directly to one of the pivot points. The gate option is used to prevent encoder outputs from changing during readout. The experiment azimuth angle is measured with respect to the local horizontal component of the Earth's magnetic field by a two-axis ring-core fluxgate magnetometer. The design of the sensor is based on probes developed at the GSFC for interplanetary missions^{14,15}. The sensor head is mounted on top of a long vertical boom in order to isolate it from gondola-induced perturbations of the local field. A second magnetometer is mounted on the gondola substructure for redundancy. The voltages in the two sense-windings of the selected magnetometer (V_x and V_y) are alternately monitored by the microcomputer through a 12-bit analog-to-digital converter.

The magnetic azimuth A_m is calculated as $A_m = \arctan (V_x/V_y)$. A magnetic offset (set by telecommand) is added to A_m to give true azimuth.

f. Ground Support Electronics

An Interdata 716 computer is used for real-time decommutation and analysis of data, as well as for digital recording of the data for later analysis. The computer receives data via CAMAC from a Goddard-built frame synchronizer. The system uses a Lear-Siegler ADM-2 terminal for operator input, a Lear Siegler ADM-1 terminal for real-time display of housekeeping data, a Tektronix 611 storage display scope for display of spectral histograms, a Versatek 800A printer/plotter for hard copy of displays, and two Wangco 1045 9-track tape drives for data recording. A Diablo Systems Model 31 disk drive is used for program storage as well as storage of accumulated detector and/or shield spectra. Commands to the gondola may be initiated under computer control (with reformatting, if necessary) and are transferred to the command transmitter via CAMAC interface.

The computer derives timing information from a time standard module identical in design to the one used in the experiment. Both clocks are recorded on the digital tape, enabling detailed monitoring of the performance of the gondola clock. Both clocks are checked against, and set with, a Goddard-built time transfer standard consisting of an Efratom model FRK precision rubidium vapor locked oscillator, clock circuitry, a battery pack and charger, and display, setting, and time code generating circuitry. The time transfer standard acquires time from a primary standard at Goddard and maintains this to an accuracy of better than 0.1 ms over a 1-month period.

III. FLIGHT PERFORMANCE

a. Flight History

Table 2 summarizes the six launches of LEGS which occurred prior to 1982. One flight was unsuccessful due to instrument problems and two others were prematurely terminated because of balloon failures. The coaxial detector system has been flown successfully twice and the planar system once. Several papers based on these observations have been published¹⁶⁻¹⁹ and others are in preparation. Some subsystems have evolved since the early flights and only the most recent versions are described in this paper.

Typically, the in-flight high-priority counting rate is ~ 10 c/s in the coaxial array (35-8000 keV) and ~ 5 c/s in the planar array (20-800 keV). Corresponding low-priority rates are ~ 350 c/s (coaxial array) and ~ 200 c/s (planar array). The NaI shield counting rate is $\sim 10,000$ c/s (≥ 80 keV). The resulting electronics deadtime is ~ 10 percent.

b. Detector Background

Due to the intense radiation environment at balloon and satellite altitudes and the weak source strengths at gamma-ray energies, observations are necessarily background dominated in this energy range. The background is substantially reduced in LEGS by the thick NaI shield that surrounds the detectors, but still the signal-to-background ratio is less than one; for instance, for a source of narrow 511-keV emission of strength 1.9×10^{-3} photons $\text{cm}^{-2} \text{s}^{-1}$ (i.e., the flux observed by HEAO-3²⁰ from the galactic center in October 1979), the LEGS coaxial signal-to-background ratio would be ~ 0.4 , yielding a measurement of $\sim 7\sigma$ significance during a typical 8-hour observation. Because of this low signal-to-background ratio, care must be

taken to ensure that the background measured during the off-source pointing is not systematically different from that measured during the on-source pointing. For example, the background pointings for the LEGS observing program were at the same elevation angle as that of the source to eliminate the observed elevation dependence of the background.

In the following three sections we discuss the background in LEGS and compare measurements of it with calculations that have been performed. The measurements for the planar array are from flight V while those for the coaxial array are from flights III and VI. The three sections cover the continuum background, the background at 511 keV, and the background at other energies at which background lines are observed. The 511-keV line is treated separately because of the different physical processes that produce background events at this energy and because of its astrophysical significance.

1) Continuum Background

The measured instrumental backgrounds for the planar and coaxial detector arrays are shown in Figures 7a and 7b, respectively. The background consists of a smooth continuum plus a number of narrow lines. The continuum is produced by three different processes, each of which dominates in a different energy range: 1) At low energies ($\lesssim 100$ keV, planar array; $\lesssim 200$ keV, coaxial array) the major source is atmospheric and cosmic gamma-rays that enter the aperture of the instrument. 2) At intermediate energies (~ 200 keV - 1 MeV) for the coaxial array the dominant source is β^- activation of the detectors themselves caused by interactions of protons and neutrons produced in the atmosphere and the shield with the nuclei of the Ge atoms. The detector signal, in this case, is due mainly to the ionization energy-loss of the β -decay electrons. 3) At high energies ($\gtrsim 100$ keV, planar array; $\gtrsim 1$ MeV, coaxial array) main component is atmospheric gamma-rays that leak through the

shield. For the planar array the shield leakage component at intermediate energies is larger than the β^- component. The increased planar shield leakage component is due to scattering in the passive iron collimator.

The calculated contribution from these components for the planar and coaxial arrays are shown as solid lines in Figures 7a and 7b, respectively. Both the aperture flux and shield leakage calculations are based on measured atmospheric and cosmic gamma-ray spectra at balloon altitudes²¹⁻²⁶. A photon/electron transport code was used to determine the detector counting rates from the spectra. The β^- -activation contribution was calculated by integrating the neutron and proton spectra at the detectors with the interaction cross-sections of each germanium isotope. The neutron and proton spectra at the detectors were determined from measured and calculated atmospheric spectra,²⁷⁻³¹ corrected for the effect of the shield. The cross-sections used were those of Silberberg and Tsao³²⁻³⁴ for proton interactions and those in references 35-38 for neutron interactions. A more detailed description of the different background components and of the calculations will be given in a future publication. The sum of all calculated components is shown as dashed lines in Figures 7a and 7b. The calculations give reasonable fits to the measured backgrounds, with typical agreement within 50 percent.

2) 511-keV Background

In addition to continuum background at 511 keV, there is also a background line at this energy as can be seen in Figures 7. There are several sources of the 511-keV background line: 1) atmospheric and cosmic 511-keV photons that enter the instrument aperture, 2) atmospheric 511-keV photons that leak through the shield without interacting in it, 3) β^+ activation due to interactions of atmospheric and cosmic-ray neutrons and protons in the

passive material inside the shield, and 4) positrons produced by pair-production interactions of atmospheric gamma-rays ($E > 1$ MeV) in the passive material inside the shield. In the cases of the β^+ -activation and pair-production positrons, the 511-keV event occurs when one of the two 511-keV photons produced by the positron annihilation is fully absorbed in a detector while the other escapes the system without triggering the shield (i.e., by shield leakage, absorption in passive material inside the shield, or escape through the aperture). Only β^+ decays in passive material inside the NaI shield contribute to the background because the energy loss of the positron itself creates a signal that either vetoes the event if the decay is in the shield, or displaces the event from the 511-keV peak if the decay is in the detector.

We performed a detailed calculation of the expected 511-keV background line intensity in the LEGS coaxial array. Because of the current interest in the 511-keV emission from the galactic center (reference 20 and references therein), the computation assumes a flight from Alice Springs, Australia (geomagnetic latitude = 32°). The gamma-ray, neutron, and proton spectra used in the calculation were the same as those used in the continuum background calculations (scaled for Alice Springs), and the interaction cross-sections were obtained from the same references as before. The angular distribution and intensity of atmospheric 511-keV photons was determined from equations and parameters given by Ling et al.³⁹ scaled for Alice Springs using HEAO-3 observations⁴⁰. The results are shown in Table 3, which lists the calculated counting rates for the various components together with their total and the measured total rate from flight VI. The almost exact agreement between calculation and measurement is fortuitous in light of the ~ 50 percent uncertainty in the calculated value. Nevertheless, the implication is that

the origin of the 511-keV background line is well understood. The calculations show that the shield leakage is the dominant component, but that the β^+ -activation and pair-production contributions are also significant.

3) Other Background Lines and the Spectrometer Resolution

A list of observed background lines and their intensities is compiled in Table 4 for both the planar and coaxial configurations. Comparable lists of background lines have been compiled for coaxial detectors on balloon flights^{3,4,5,41} and on satellites^{8,42,43}. Proctor et al.⁷ presented a short list of lines observed with a balloon-borne planar Ge array. Although a few lines can be attributed to naturally occurring radioisotopes in the gondola, the majority result from activation of the detectors and/or the surrounding material by particle radiation. On satellites, the particles responsible are cosmic ray and trapped protons⁴⁴, while on balloons the particles are mostly secondary neutrons produced in the atmosphere and the shield⁴¹.

The strongest lines (aside from the annihilation line) are due to decay of metastable levels in Ge with lifetimes $\geq 10 \mu\text{s}$. The 54 and 67 keV features mentioned in Section II d are of this type. The 23 keV line in the planar detectors may also be explained by this mechanism, but it has not been reported in previous line lists from astrophysical instruments because of either low sensitivity or high background in this energy region. Bunting and Kraushaar⁴⁵ observed a line at that energy in laboratory irradiation of a Ge detector by $\sim 10 \text{ MeV}$ neutrons. The line presumably originates from $^{71\text{m}}\text{Ge}$, where the 198 keV level has a lifetime of 22 ms and decays via an intermediate level at 175 keV. The strong 198 keV line is thus a sum peak and the 23 keV line represents the case where the 175 keV photon escapes from the detector but is not detected by the shield (otherwise the event would be vetoed). A

difficulty with this explanation is that inspection of the spectrum of low-priority events (i.e., those which have coincident shield triggers) shows little evidence for a line at this energy. The formal result for the low-priority line intensity is 0.066 ± 0.042 c/s compared to a rate of 0.129 ± 0.008 c/s in the high-priority spectrum. This implies that if the hypothesized origin is correct, ≤ 50 percent of the escaping 175 keV photons trigger the anticoincidence shield. Rough estimates of the expected rate are only marginally compatible with this number, but detailed calculations have not been performed. Better measurements are expected in a future flight.

The fact that the various isotopes of Ge have a number of long-lived isomeric states makes the NaI shield ineffective in eliminating many of the strong lines from the background spectrum because the anticoincidence gate time is shorter than the isomeric lifetime. The ^{71m}Ge and ^{73m}Ge decays also involve cascades through an intermediate level. In the case of ^{73m}Ge this effect is readily apparent because the half-life of the intermediate level (3 μs) is comparable to the resolving time (~ 5 μs) of the Ge ADC's. Thus, the background spectrum contains a line at 54 keV (due to those decays which took long enough to enable resolution of the pulses from the two cascade photons), a line at 67 keV (due to those decays where the cascade photons were sufficiently close in time to sum together in the ADC), and an additional component in the continuum between 54 and 67 keV (due to partial summing of the two pulses). This is illustrated in Figure 8a, which shows a background spectrum from the planar detector array. The lines at 23, 93, 140, and 198 keV are also prominent.

The PPT circuit described in Section II d was installed to take advantage of the fact that pulse pairs separated by ~ 3 μs are a statistically improbable occurrence unless they are correlated as in the ^{73m}Ge decay. Thus, elimination of closely-spaced pairs tagged as such by the PPT circuit removes

only the features associated with the ^{73}Ge decays. A spectrum with all pulse pairs closer than 20 μs removed is shown in Figure 8b. The PPT is very successful at removing the 54 keV line and the continuum of partially-summed ^{73}Ge events, but the 67 keV line is mostly unaffected. The 54 keV rate in Figure 8a is $(1.5 \pm 0.1) \times 10^{-1}$ c/s, compared with a 2σ upper limit of 8×10^{-3} c/s in Figure 8b. The performance is approximately as expected, given the resolving-time limitations of the PPT. It is anticipated that future improvements in the PPT design will also enable reduction of the 67 keV feature as well. Nevertheless, the removal of a significant source of background (and possible systematic errors) from the region between 50 and 65 keV is an important success for observations of spectral features such as that reported^{13,16} in the spectrum from Her X-1.

We noted earlier that the resolution for the entire array is generally worse than the figures quoted for single detectors in the laboratory. Two effects are primarily responsible for this: 1) the PHA conversion parameters are temperature dependent; and 2) the differential and integral non-linearities of the PHA system are different in detail for the three detectors. Although partial compensation for these effects can be accomplished in the post-flight analysis, complete compensation is impractical. Furthermore, in the case of the coaxial array, the PHA channel width is a substantial fraction of the peak width; thus, quantization errors are also important and complete compensation for these is impossible.

Because of the effect of thermal drifts, the attainable resolution varies slightly from one observation to the next. Nevertheless, we quote typical values for an 8-hour observation derived from measurements of the background lines in flights III and V. For the coaxial detectors the resolution (FWHM) varies from 1.8 keV at 70 keV to 3.5 keV at 2.6 MeV; in the

region around 500 keV $E_{FWHM} = 2.2$ keV. For the planar detectors $E_{FWHM} = 1.4$ keV over the entire region from 20-200 keV.

IV. SENSITIVITY

The normal procedure for observing a source with LEGS is to alternate between target and background intervals every 20 minutes. During the background intervals, the telescope axis is maintained at the same elevation angle as the source but is offset in azimuth by an amount large enough to ensure that the source is outside the telescope field-of-view. For the coaxial detectors this usually means that the azimuth offset is 180° , although smaller values have been used when the source elevation was sufficiently low. For the planar detectors, an azimuth offset of 30° is used when the source elevation is $< 65^\circ$. In all cases where the offset is less than 180° , the background offsets are alternately clockwise and counterclockwise from the source direction. For each target interval, subtraction of background from preceding and succeeding intervals minimizes systematic errors from any east-west azimuthal anisotropy as well as any elevation dependence of the background. The sensitivity calculations which we report in this section are purely statistical and do not include any residual systematic errors from these (or other) effects.

Figure 9 shows the narrow-line sensitivity curves for both LEGS configurations for a 3σ level of confidence. The curves are based on the formula of Jacobson et al.⁴ and represent the performance attainable on a typical balloon flight from Palestine, Texas. The source is assumed to transit nearly overhead (i.e., source declination δ such that $20^\circ \lesssim \delta \lesssim 40^\circ$) and the residual atmospheric depth is assumed to be ~ 3 g/cm². Observations

are performed while the source elevation is $> 30^\circ$, so that the assumed time on source is $\sim 15,000$ s with an equal time off-source.

Several comments on Figure 9 are relevant:

1. It is readily apparent that the advantage of the planar array over the coaxial array extends up to ~ 200 keV.
2. The calculation implicitly assumes that no continuum flux is observed from the hypothetical target. If, as in the case of the Crab nebula, there is significant continuum flux, then this flux is effectively an additional background component in the search for emission lines. Thus, for the same conditions, the sensitivity to narrow lines from such a source will be worse than shown in Figure 9 (cf. reference 17).
3. The search for a line from a source which is known to pulsate can have better sensitivity to narrow lines because the off-pulse portion of the observation can be used as background and/or because the limits are quoted as time-averaged rate rather than an instantaneous rate.
4. If the line is assumed to be much broader than the resolution of the instrument, the sensitivity curves must be increased by approximately the square root of the ratio of the line width to the instrumental resolution.

The gaps in the curves in Figure 9 represent regions where the presence of strong background lines causes a substantial increase in the minimum detectable line flux. The most astrophysically interesting of these is the 511-keV e^+e^- annihilation line. For this case, we have calculated the sensitivity using the same assumptions as for the curves in Figure 9, except that the background flux values are those achieved in flight VI, from Alice Springs, Australia. This is because the line has been previously observed (see reference 20 and references therein) to emanate from the region of the Galactic Center, which is observable from the southern hemisphere. Since this

case involves a search for a line at an a priori astrophysically interesting energy, the 2σ confidence level is appropriate, for which the sensitivity limit is 5.9×10^{-4} ph/cm²-s.

V. CONCLUSIONS

The LEGS instrument achieves very good sensitivity to narrow line emission from astrophysical sources over the energy range from 20 to 8000 keV. The relative simplicity of the design has facilitated our understanding of the instrumental response and background properties which will be important in the future development of more sensitive instruments. Design optimizations at energies below a few hundred keV are not only different from, but sometimes in opposition to, design optimizations at higher energies. This is illustrated by the fact that the passive collimator, which provides better angular resolution and reduces the aperture component of the background flux for the planar array, causes an increase in the 511-keV line background by adding to both the β^+ activation and pair-production components. Development of a single, wideband instrument to cover the entire 20-8000 keV range is thus technically more complicated and probably involves compromises in performance relative to separate configurations.

The LEGS telescope concept is straightforward and the analysis required to deconvolve the source is relatively simple. Although significant improvements in sensitivity and angular response could be achieved by simply scaling up the LEGS design, this approach would certainly lead to a rather large and costly instrument. Innovations in experiment design, particularly with regard to the suppression of background, are therefore of paramount importance. The experience gained with LEGS has, in fact, pointed the way towards a number of new techniques that have the potential of accomplishing this objective.

ACKNOWLEDGEMENTS

Many people have made important contributions to the LEGS program during its history, and we can only acknowledge a few by name. W. K. H. Schmidt made many scientific contributions to the design phase and the first few flights. Essential software support was provided through the efforts of D. Argo, H. Eisericke, A. Engel, and N. Laubenthal. S. Derdyn contributed the mechanical design of the azimuth drive system and R. Hoffman aided in the thermal analysis of the system. We also thank J. Newby for typing the manuscript of this paper.

REFERENCES

1. R. E. Lingenfelter and R. Ramaty, *Physics Today* 31 (1978) No. 3, 40.
2. A. S. Jacobson, Ph. D. Thesis, UCSD SP-68-2 (1968).
3. E. A. Womack and J. W. Overbeck, *J. Geophys. Res* 75 (1970) 1811.
4. A. S. Jacobson, R. J. Bishop, G. W. Culp, L. Jung, W. A. Mahoney, and J. B. Willett, *Nucl. Instr. and Meth.* 127 (1975) 115.
5. M. Leventhal, C. MacCallum, and A. Watts, *Astrophys. J.* 216 (1977) 491.
6. F. Albernehe, D. Boclet, J. P. Chabaud, J. Claisse, Ph. Durouchoux, P. Frabel, E. Olivier, J. M. da Costa, P. Pagnier, R. Rocchia, and G. Vedrenne, *Nucl. Instr. and Meth.* 155 (1978) 171.
7. R. Proctor, W. Pietsch, and C. Reppin, *Nucl. Instr. and Meth.* 197 (1982) 477.
8. G. H. Nakano, W. L. Imhof, J. B. Reagan, and R. G. Johnson, in "Gamma-Ray Astrophysics", ed. F. W. Stecker and J. I. Trombka, NASA SP-339 (1973) 71.
9. G. H. Nakano and W. L. Imhof, in "Gamma Ray Spectroscopy in Astrophysics", ed. T. L. Cline and R. Ramaty, NASA TM-79619 (1978) 529.
10. W. A. Mahoney, J. C. Ling, A. S. Jacobson, and R. M. Tapphorn, *Nucl. Instr. and Meth.* 178 (1980) 363.
11. T. W. Randorf, R. C. Trammell, and L. S. Darken, Jr., *IEEE Trans. Nucl. Sci.* NS-26 (1979) 297.
12. C. M. Lederer and V. S. Shirley, eds. "Table of Isotopes", Seventh Edition (Wiley and Sons, New York: 1978) 239.
13. J. Trümper, C. Reppin, W. Voges, R. Staubert, and E. Kendziorra, *Astrophys. J.* 219 (1978) L105.

14. M. H. Acuna and C. J. Pellerin, IEEE Trans. Geo. Electronics GE-7 (1969) 252.
15. M. H. Acuna, IEEE Trans. Magnetics MAG-10 (1974) 519.
16. J. Tueller, T. Cline, W. Paciasas, B. Teegarden, D. Boclet, P. Durouchoux, J. Hameury, and R. Haymes, Proc. 17th Intl. Cosmic Ray Conference, Paris, Vol. 1 (1981) 95.
17. J. M. Hameury, D. Boclet, Ph. Durouchoux, T. Cline, W. Paciasas, B. Teegarden, J. Tueller, and R. Haymes, Proc. 17th Intl. Cosmic Ray Conference, Paris, Vol. 9 (1981) 21.
18. W. S. Paciasas, T. L. Cline, B. J. Teegarden, J. Tueller, P. Durouchoux, and J. M. Hameury, in "The Galactic Center", ed. G. R. Riegler and R. D. Blandford (Am. Inst. Phys., New York: 1982) 139.
19. _____, Astrophys. J. 260 (1982) L136.
20. G. R. Riegler, J. C. Ling, W. A. Mahoney, W. A. Wheaton, J. B. Willett, A. S. Jacobson, and T. A. Prince, Astrophys. J. 248 (1981) L13.
21. R. L. Kinzer, W. N. Johnson, and J. D. Kurfess, Astrophys. J. 222 (1978) 370.
22. V. Schönfelder, U. Graser, and J. Daugherty, Astrophys. J. 217 (1977) 306.
23. V. Schönfelder, F. Graml, and F.-P. Penningsfeld, Astrophys. J. 240 (1980) 350.
24. J. C. Ling, J. Geophys. Res. 80 (1975) 3241.
25. C. E. Fichtel, G. A. Simpson, and D. J. Thompson, Astrophys. J. 222 (1978) 833.
26. M. V. Zombeck, Smithsonian Astrophysical Observatory Special Report No. 386 (1980) 3.

27. T. W. Armstrong, K. C. Chandler, and J. Barish, *J. Geophys. Res.* 78 (1973) 2715.
28. A. M. Preszler, G. M. Simnett, and R. S. White, *J. Geophys. Res.* 79 (1974) 17.
29. K.-P. Wenzel, E. C. Stone, and R. E. Vogt, *J. Geophys. Res.* 80 (1975) 3580.
30. B. J. Teegarden, *J. Geophys. Res.* 72 (1967) 4857.
31. F. B. McDonald, *Phys. Rev.* 115 (1959) 194.
32. R. Silberberg and C. H. Tsao, *Astrophys. J. Suppl.* 25 (1973) 315.
33. _____, *Astrophys. J. Suppl.* 25 (1973) 335.
34. _____, *Proc. 15th Intl. Cosmic Ray Conference, Vol. 2* (1977) 84.
35. R. J. Howerton, R. E. Dye, and S. T. Perkins, LLNL Report UCRL-50400, Vol. 18, Rev. 1 (1982), to be published.
36. D. I. Garber and R. R. Kinsey, BNL Report No. 325, 3rd Ed., Vol. 2 (1976).
37. "Handbook on Nuclear Activation Cross-Sections", Intl. Atomic Energy Agency, Tech. Report Series No. 156 (Vienna: 1974).
38. W. E. Alley and R. M. Lessler, LLNL Report UCRL-50484, Rev. 1 (1972).
39. J. C. Ling, W. A. Mahoney, J. B. Willett, and A. S. Jacobson, *J. Geophys. Res.* 82 (1977) 1463.
40. W. A. Mahoney, J. C. Ling, and A. S. Jacobson, *J. Geophys. Res.* 86 (1981) 11098.
41. W. A. Mahoney, J. C. Ling, J. B. Willett, and A. S. Jacobson, in "Gamma Ray Spectroscopy in Astrophysics", ed. T. L. Cline and R. Ramaty, NASA TM-79619 (1978) 462.
42. G. H. Nakano, W. L. Imhof, and R. G. Johnson, *IEEE Trans. Nucl. Sci.* NS-21 (1974) 159.

43. W. A. Mahoney, private communication (1980).
44. W. A. Mahoney, J. C. Ling, and A. S. Jacobson, Nucl. Inst. and Meth. 185
(1981) 449.
45. R. L. Bunting and J. J. Kraushaar, Nucl. Inst. and Meth. 118 (1974) 565.

TABLE 1

LEGS Germanium Detector Characteristics

	<u>Coaxial Array</u>	<u>Planar Array</u>
Crystal Dimensions	5 cm diameter x 4.6 cm thick	5 cm diameter x 1 cm thick
Bias Voltage	+ 1500 v	- 1500 v
Active Volume (Total)	230 cm ³	57 cm ³
Effective Area (Maximum)	35.5 cm ² (E ~ 130 keV)	53 cm ² (E ≤ 100 keV)
Laboratory Resolution (FWHM)	1.6 keV at 60 keV 1.8 keV at 662 keV 2.5 keV at 2614 keV	0.9 keV at 60 keV 1.0 keV at 122 keV
Cryostat Window Thickness	0.17 cm Al	0.05 cm Be

TABLE 2
LEGS Flight History

<u>Flight Number</u>	<u>Launch Site and Local Date</u>	<u>Detector Configuration</u>	<u>Float Duration (Hours)</u>	<u>Targets Observed</u>	<u>Notes</u>
I	1978, October 17 Palestine, Texas	Coaxial	14	--	Instrument problems precluded observations
II	1979, May 13 Palestine, Texas	Coaxial	--	--	Leaky balloon; failed to ascend above 90,000 feet.
III	1979, May 25 Palestine, Texas	Coaxial	9	Galactic Plane Cas A	
IV	1980, May 9 Palestine, Texas	Planar	--	--	Leaky balloon; failed to ascend above 75,000 feet
V	1980, Sept. 24 Palestine, Texas	Planar	22.5	Her X-1 Cyg X-1 Crab Nebula A0535+26	
VI	1981, Nov. 20 Alice Springs, Australia	Coaxial	11	Cen A Galactic Center	

TABLE 3
Calculated 511-keV Counting Rate in Alice Springs

<u>Origin</u>	<u>Count Rate</u> (counts/second)
Aperture Flux (16° FWHM)	7.8×10^{-4}
Shield Leakage	1.8×10^{-2}
β^+ Activation	7.7×10^{-3}
Pair Production	6.0×10^{-3}
 Total Calculated	 $3.2 \times 10^{-2*}$
Total Measured	$3.5 \times 10^{-2**}$

* Typical uncertainty = 50 percent. The continuum contribution is not included in either the calculated or measured number. Continuum background in a 3-keV interval at 511 keV is $\sim 1.1 \times 10^{-2}$ c/s.

** The measured value in Palestine (flight III) is 7.9×10^{-2} c/s. Direct comparison is complicated by the difference in typical float altitudes (5.0 g/cm²-flight III, 3.5 g/cm²-flight VI), and the difference in shield threshold (~ 100 keV-flight III, ~ 50 keV-flight VI).

TABLE 4

LEGS Background Lines

Energy (± 1 keV)	Coaxial Intensity (10^{-3} counts/second)	Planar Intensity (10^{-3} counts/second)	Probable Origin
23	Note 1	129 \pm 8	^{71m}Ge (Detectors)
54	584 \pm 10	Note 2	^{73m}Ge (Detectors)
67	669 \pm 10	129 \pm 7	^{73m}Ge (Detectors)
93	19 \pm 6	24 \pm 6	^{67m}Zn (Detectors) ?
140	378 \pm 8	100 \pm 5	^{75m}Ge (Detectors)
160	10 \pm 5	10 \pm 3	^{77m}Ge (Detectors)
175	41 \pm 5	7 \pm 2	^{71m}Ge (Detectors)
186	27 \pm 4	10 \pm 3	^{66}Cu (Cold Finger) ?
198	651 \pm 9	130 \pm 5	^{71m}Ge (Detectors)
212	10 \pm 4	10 \pm 3	^{121}I (Shield)
239	27 \pm 4	14 \pm 3	^{212}Pb (Natural)
352	7 \pm 3	< 4	^{214}Pb (Natural)
418	7 \pm 3	< 4	?
440	21 \pm 3	10 \pm 4	$^{23*}\text{Na}$ (Shield) ?
473	32 \pm 3	8 \pm 2	^{24m}Na (Al Housings)
497	9 \pm 3	4.9 \pm 1.4	^{115}Sb (Shield)
511	79 \pm 5	21 \pm 3	e^+e^- Annihilation
583	7 \pm 2	< 3	^{208}Tl (Natural)
844	32 \pm 3	Note 3	$^{27*}\text{Al}$ (Al Housings)
969	12 \pm 2	Note 3	^{228}Ac (Natural)
1015	16 \pm 2	Note 3	$^{27*}\text{Al}$ (Al Housings)
1369	4.6 \pm 1.4	Note 3	^{24}Na (Al Housings, Shield)
1461	6.1 \pm 1.4	Note 3	^{40}K (Natural)
1633	4.0 \pm 1.3	Note 3	^{20}F (Al Housings)
1779	3.9 \pm 0.8	Note 3	^{28}Al (Al Housings)
2615	3.4 \pm 0.5	Note 3	^{208}Tl (Natural)

Note 1. Below lower detector threshold
 Note 2. See Section IIIb, Part 3
 Note 3. Above upper detector threshold

FIGURE CAPTIONS

- Figure 1. Side view of LEGS from a direction perpendicular to the elevation axis of rotation. Major components of the instrument are labeled.
- Figure 2. The effective area of the LEGS detector arrays over their operating range. Coaxial K-escape and single- and double-511 keV escape peaks are not shown because they are less than 0.1 cm^2 . The curves represent the response to an on-axis parallel beam and are derived from laboratory measurements and Monte Carlo computer simulations.
- Figure 3. Comparison of the two LEGS detector configurations. Primary components of the instrument are shown to scale with their actual relative separations. Shield and cryostat housings and electronics are not included.
- Figure 4a. Summed angular response of the LEGS coaxial configuration. The solid line and long-dashed line represent the extremes of asymmetry which occur every 30° in azimuth around the collimator axis. In the most asymmetric case (solid line) the contributions of individual detectors are readily apparent. The curves are computer simulations which have been adjusted to fit laboratory measurements at 662 keV. The short-dotted lines represent the broadening in the wings which occurs at higher energies ($\sim 1200 \text{ keV}$) and for the Compton continuum.

Figure 4b. Angular response of the LEGS planar configuration. The curves are computer simulations which have been checked with laboratory measurements at 60 keV. The extreme cases of the response parallel to (dashed line) and perpendicular to (solid line) the central iron slat are shown. The effect of the NaI active collimator is negligible except for the introduction of a slight asymmetry in one wing of the dashed line for offset angles $\geq 5^\circ$.

Figure 5. Block diagram of the instrument electronics. Commercial NIM modules are used for the Ge spectroscopy amplifiers and 8192-channel ADCs. Ge preamplifiers are modified commercial units. The remaining components are custom designs. The pulse-pair timing (PPT) circuit (see text) is shown as a dashed line because it has been used only in the planar configuration.

Figure 6. Block diagram of the pointing system electronics. The microprocessor calculates the desired values of elevation and azimuth, compares these with actual values, and drives control motors appropriately. Two cross magnetometers are flown for redundancy. Selection of the one to be used is performed by telecommand from the ground.

Figure 7a. Measured and calculated continuum background in the planar array. The data are from flight V (Palestine, Texas; residual atmosphere $\sim 4 \text{ g/cm}^2$). The aperture flux, β^- decay, and shield leakage components of the calculated background are shown separately as solid lines. The dashed line represents the sum of

these components. The typical uncertainty in the calculations is 50 percent.

Figure 7b. Measured and calculated continuum background in the coaxial array. The data are from flight III (Palestine, Texas; residual atmosphere $\sim 5 \text{ g/cm}^2$). The calculated components are represented in the same way as in Figure 7a.

Figure 8. a) Inflight background spectrum from the planar array with the PPT circuit disabled. The lines at 54 and 67 keV from $^{73\text{m}}\text{Ge}$ are prominent, as is the increased continuum between the lines due to partial summing of the cascade photons. b) The same spectrum is shown with the PPT circuit eliminating all pulse pairs closer than 20 μs . The 54 keV line is negligible, as is the continuum of partially summed events. The 67 keV line is mostly unaffected because of resolving time limitations of the PPT circuit.

Figure 9. Sensitivity of LEGS to narrow lines at the 3σ confidence level on a typical one-day balloon flight. Gaps in the curves indicate the vicinity of strong background features where the attainable sensitivity would be significantly worse. The assumptions used in deriving these curves are described in the text.

ORIGINAL PAGE IS
OF POOR QUALITY

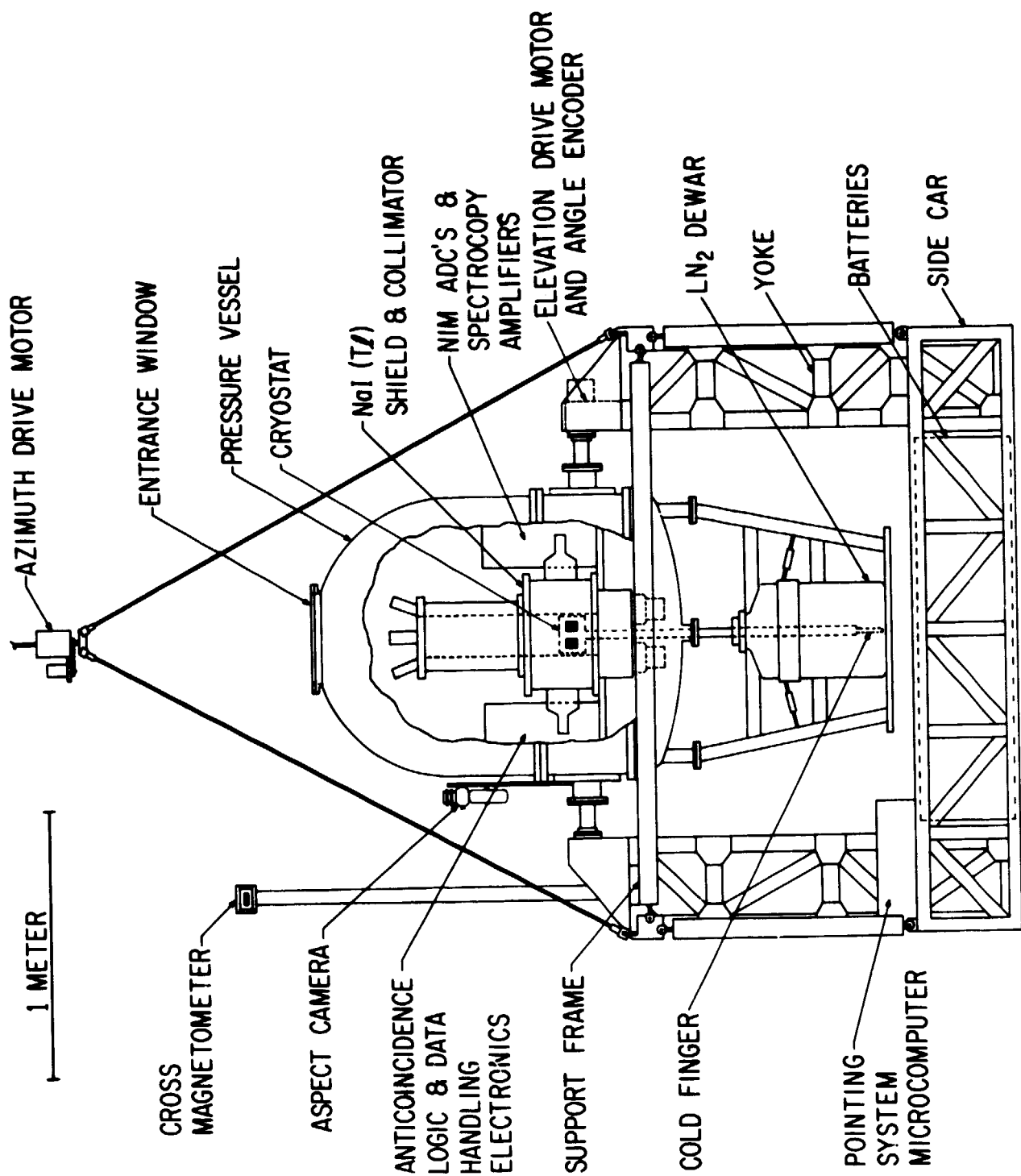


Fig.1

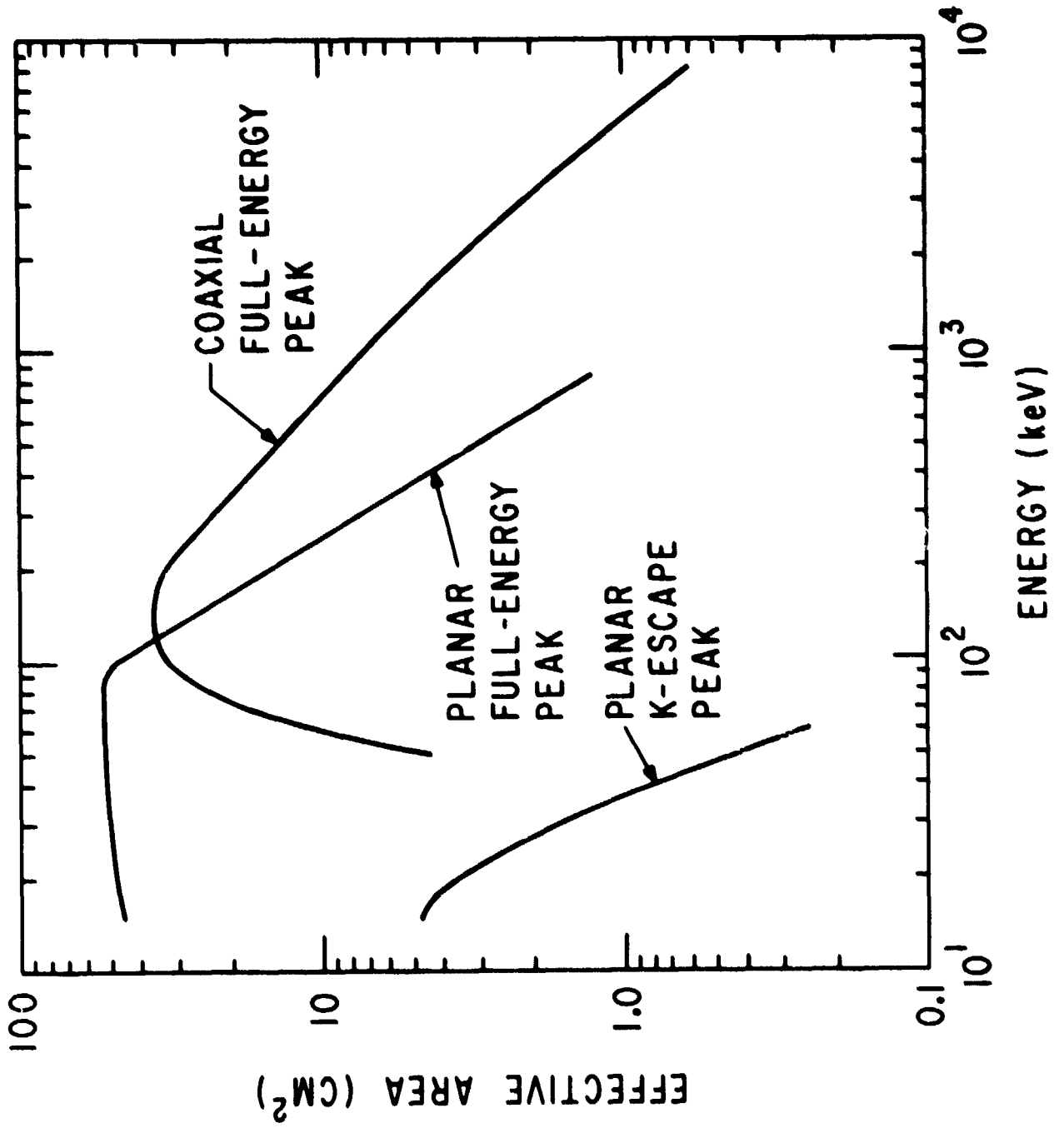


FIG. 2

ORIGINAL PAGE IS
OF POOR QUALITY

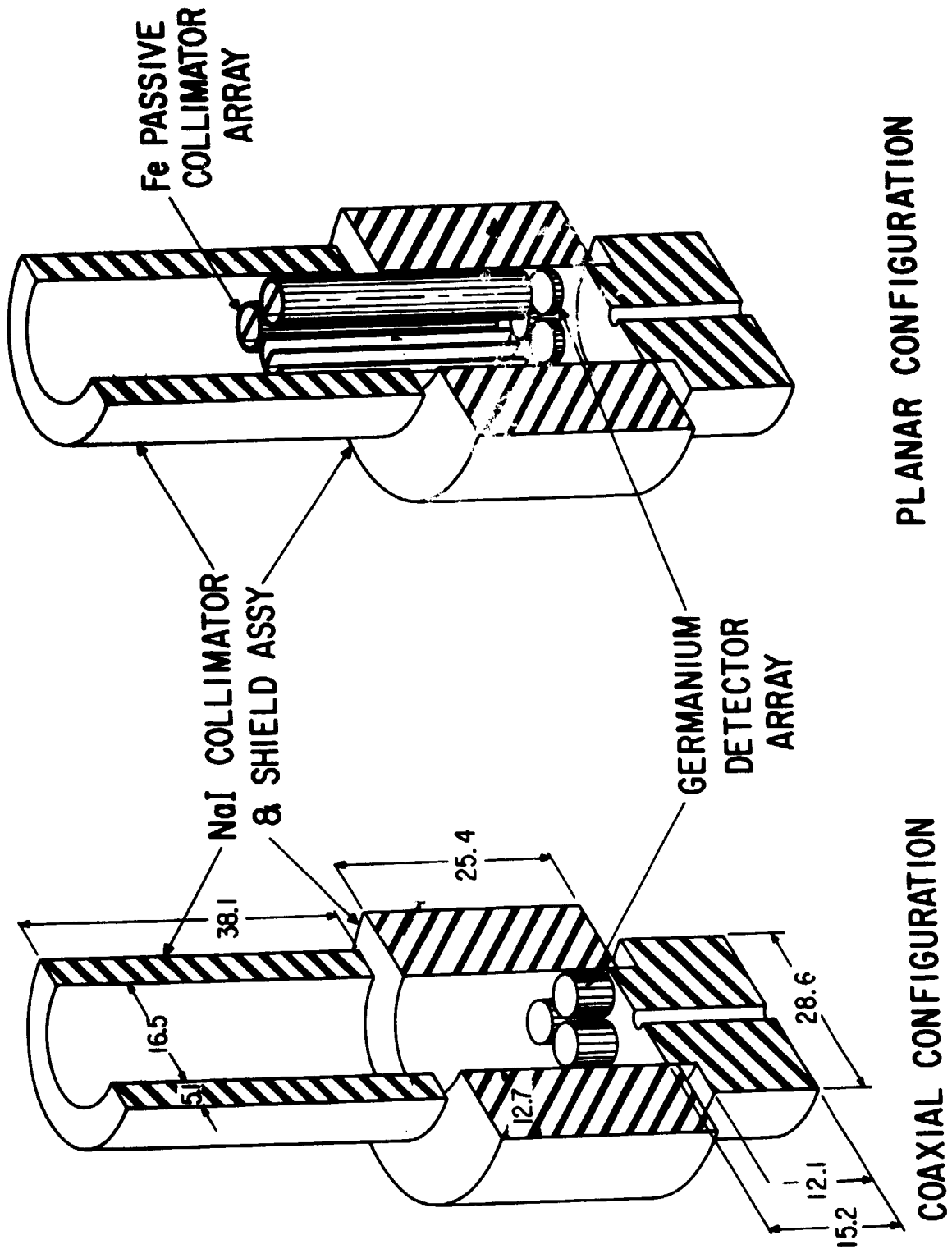


Fig.3

ORIGINAL PAGE IS
OF POOR QUALITY

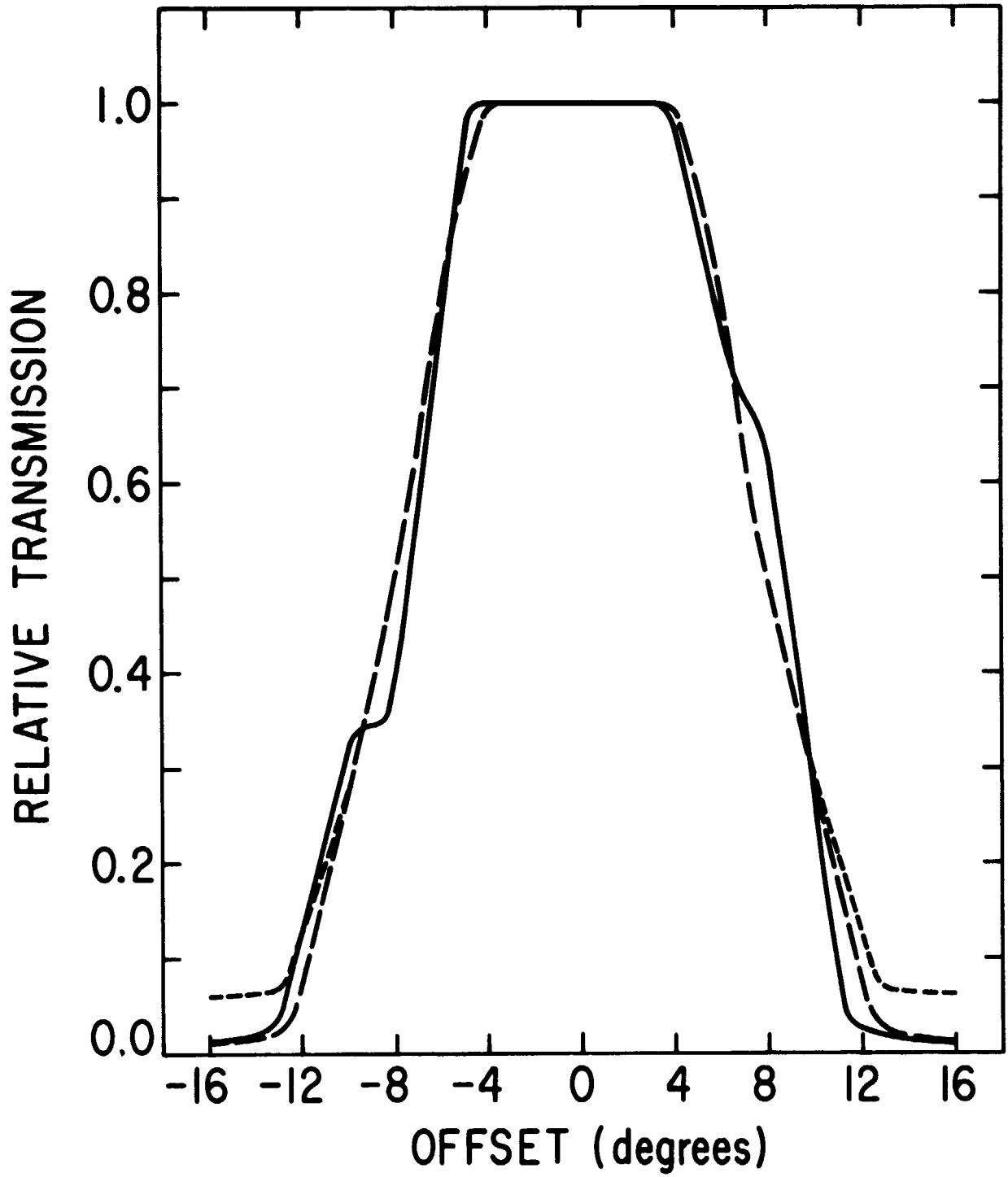


Fig.4a

ORIGINAL PAGE IS
OF POOR QUALITY

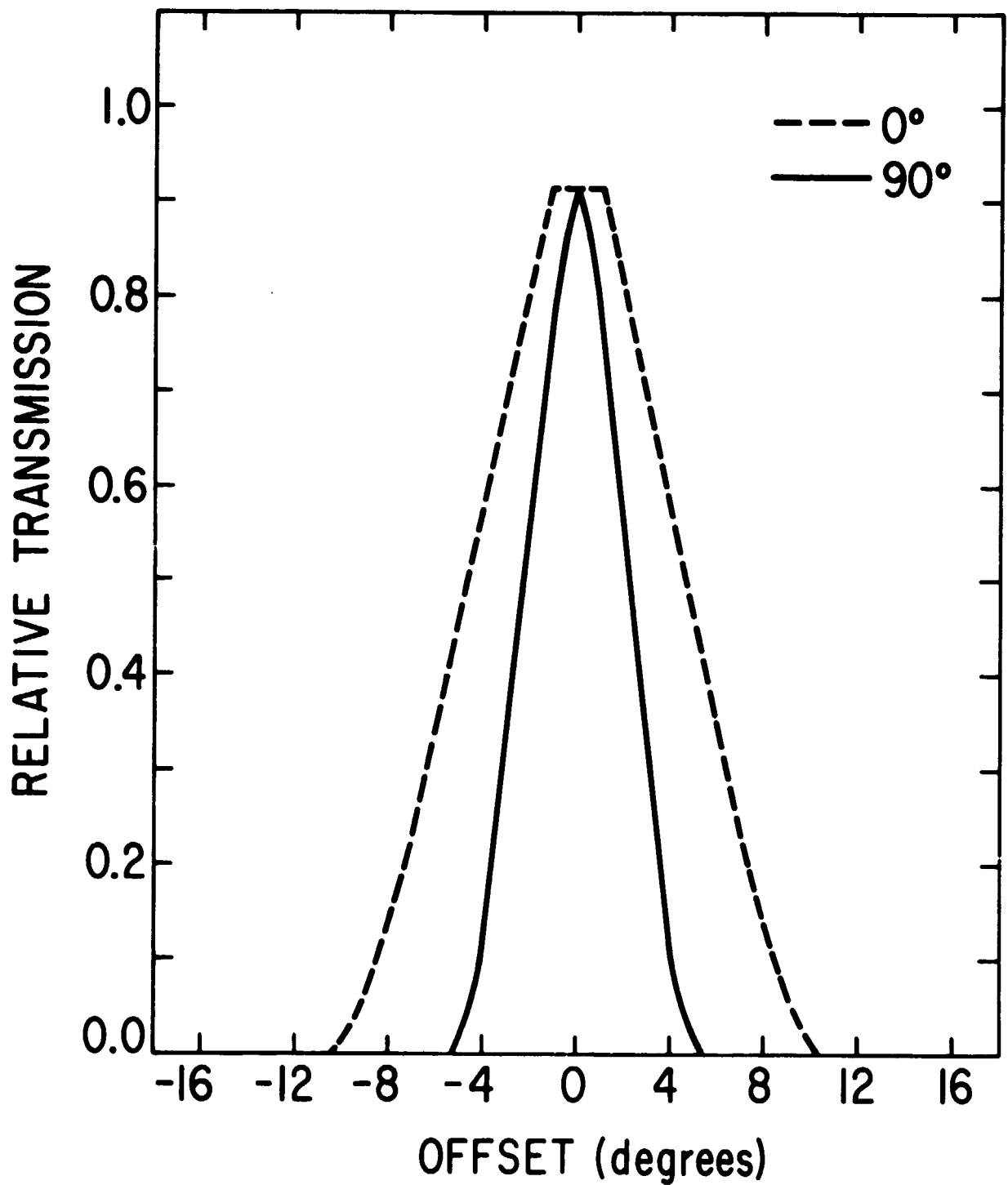


Fig.4b

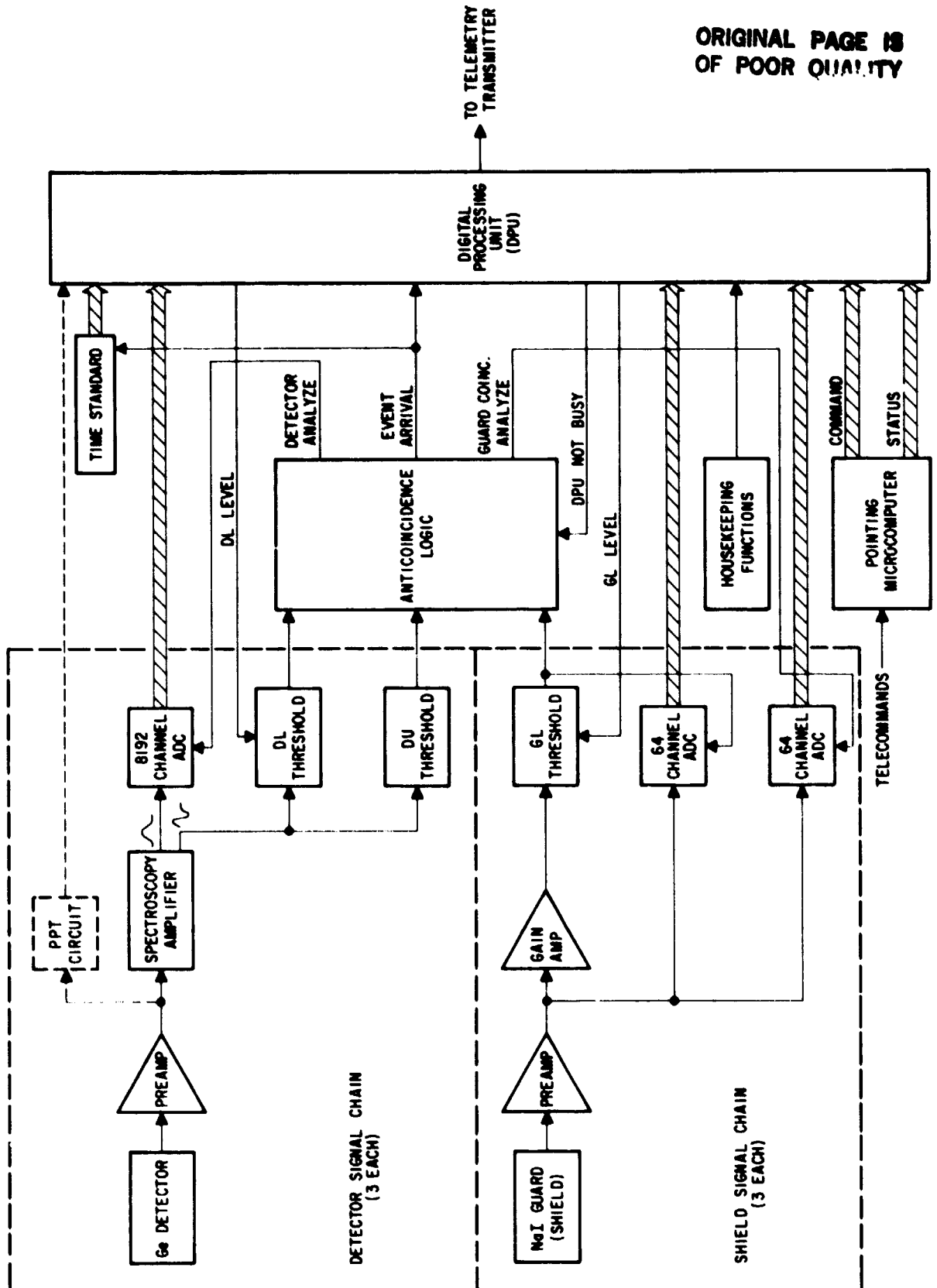


Fig. 5

ORIGINAL PAGE IS
OF POOR QUALITY

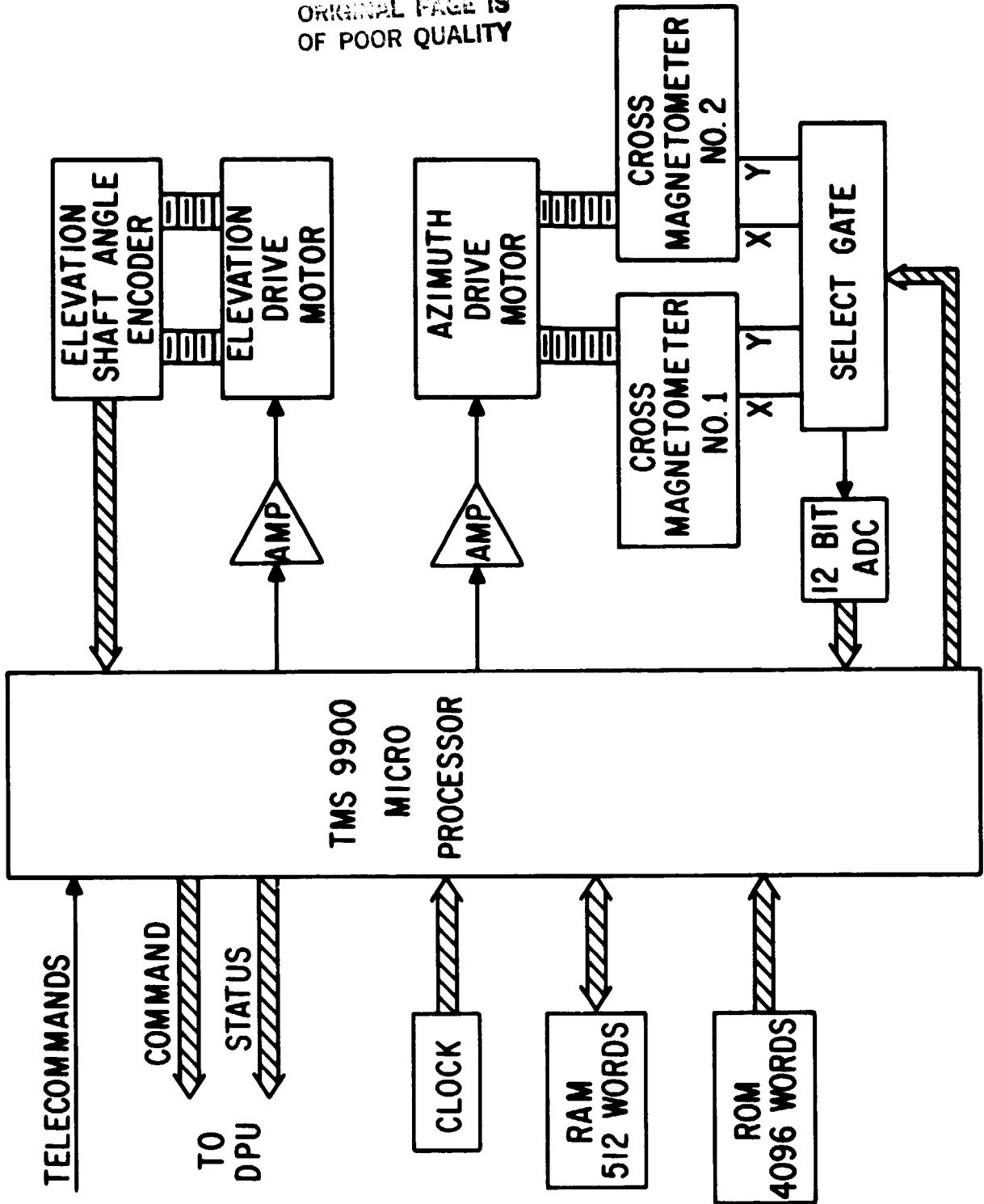


Fig. 6

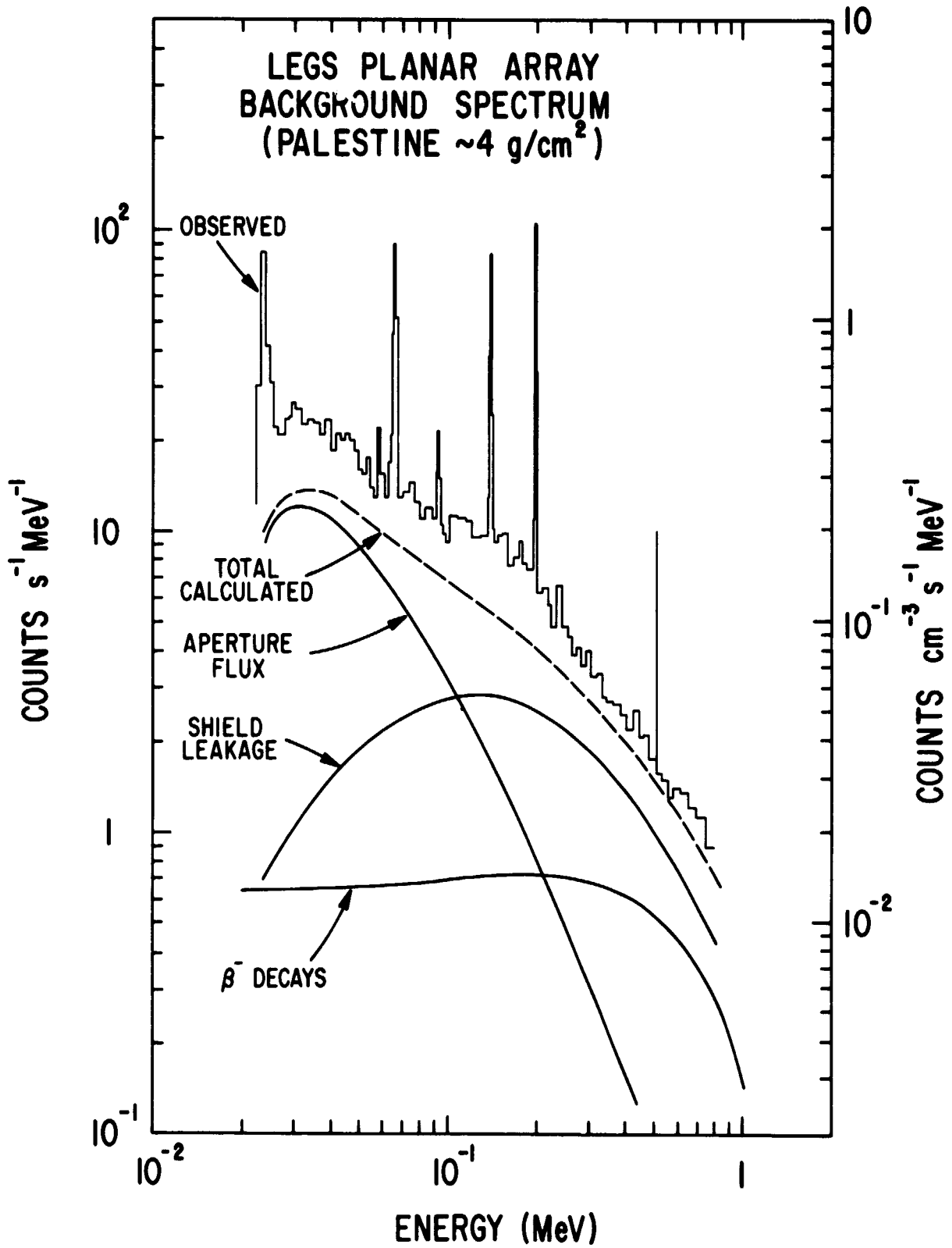


Fig. 7a

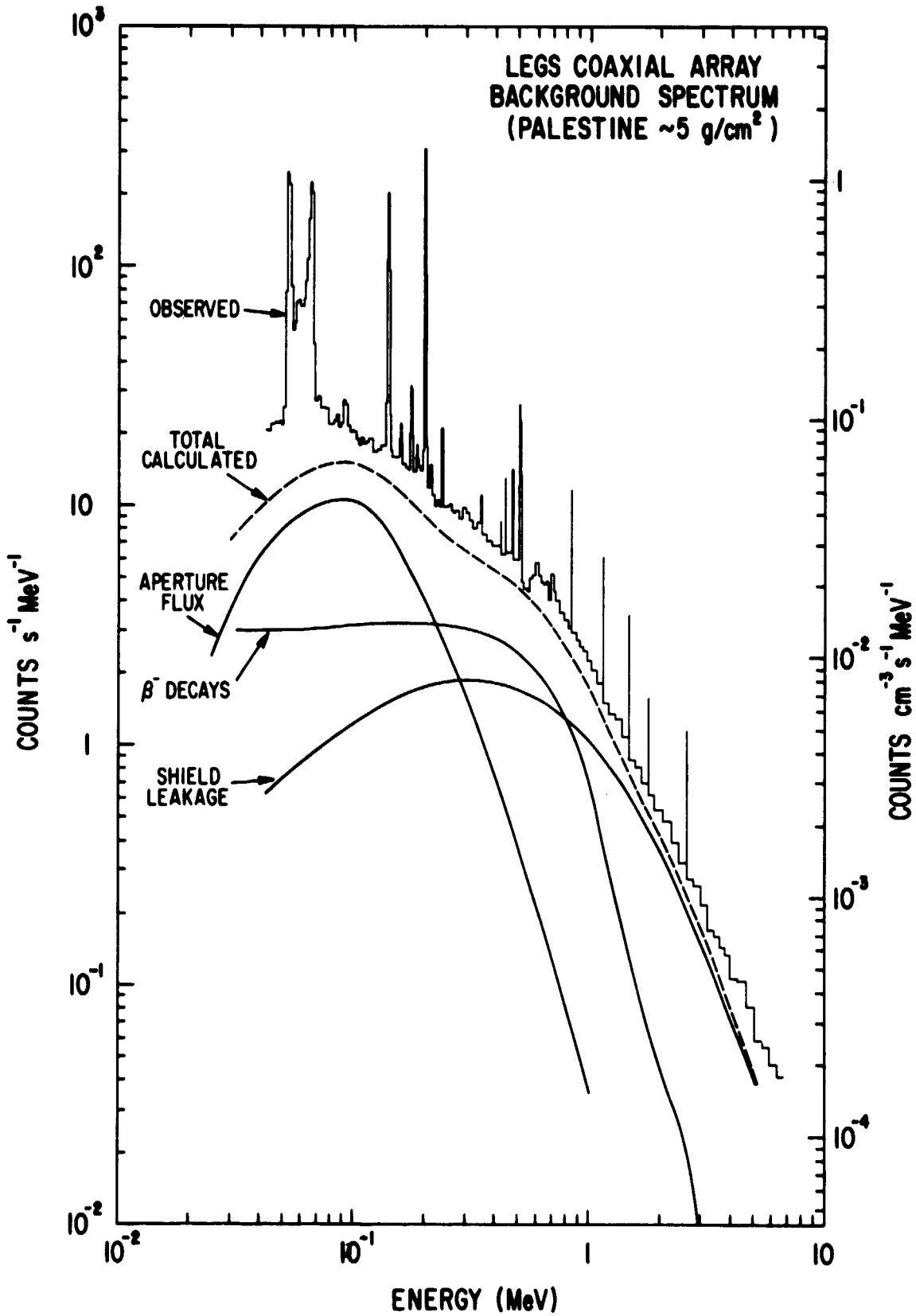


Fig. 7b

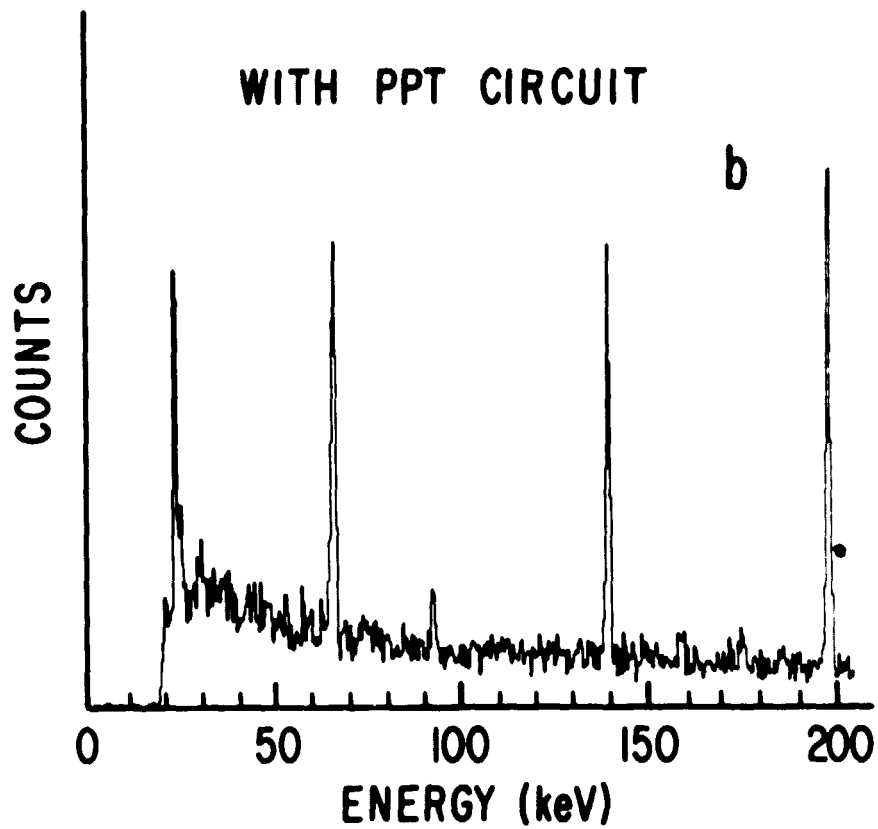
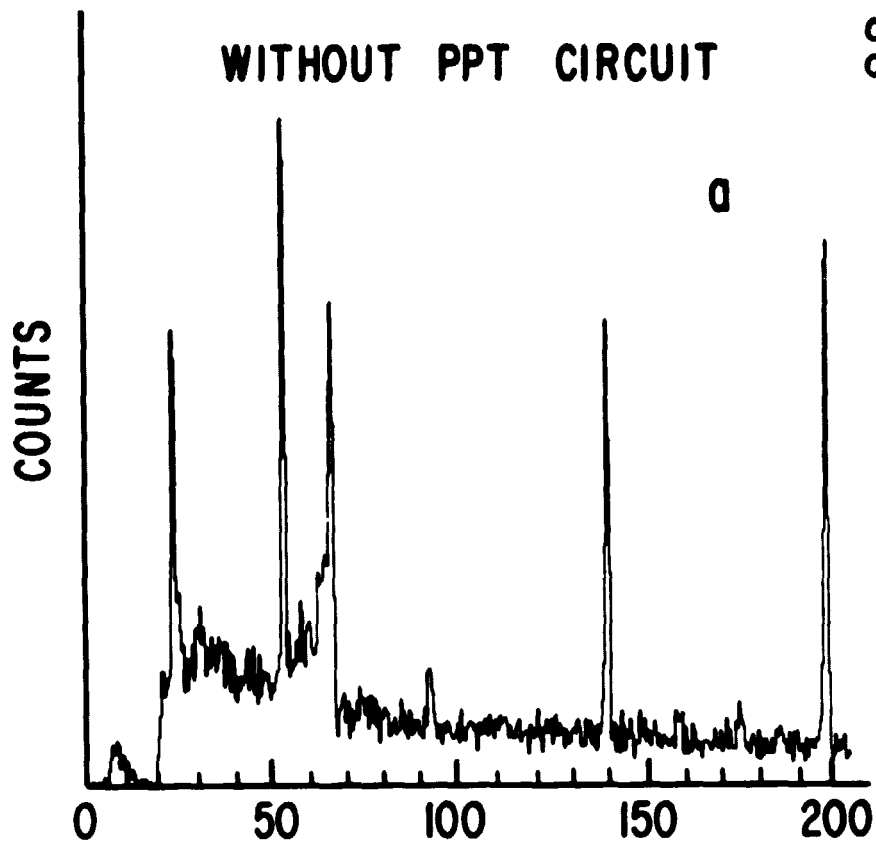


Fig. 8

ORIGINAL PAGE IS
OF POOR QUALITY.

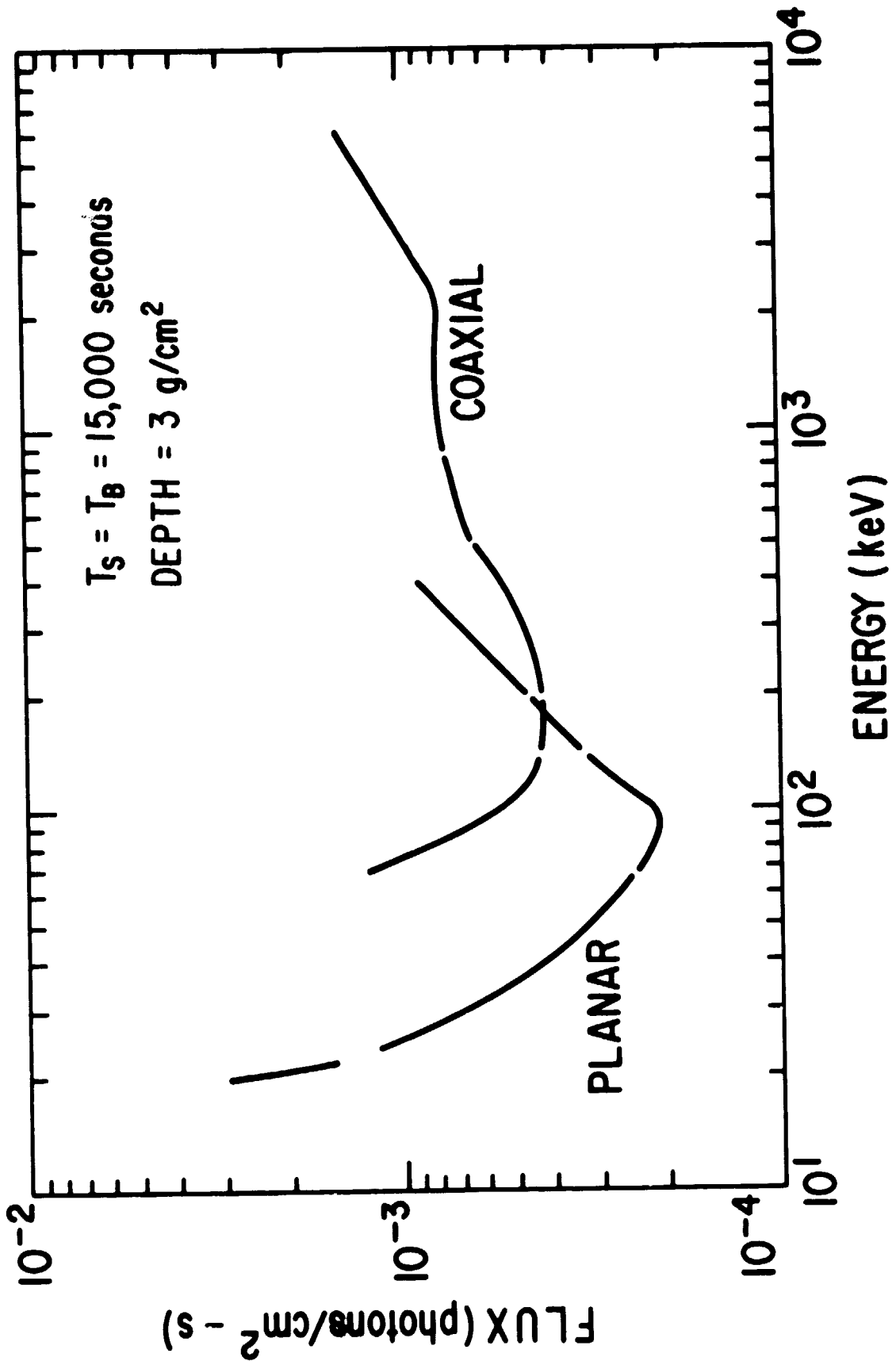


Fig. 9